Iterative Frequency-Domain Joint Channel Estimation and Data Detection of Faster-Than-Nyquist Signaling

Takumi Ishihara, *Student Member, IEEE*, and Shinya Sugiura, *Senior Member, IEEE*

***Abstract*— In this paper, we propose semi-blind iterative frequency domain joint channel estimation (CE) and data detection (DD) of faster-than-Nyquist signaling (FTNS). The proposed scheme achieves low-complexity operation, while maintaining a performance close to that of the perfect channel state information scenario. More specifically, we derive low-complexity frequency-domain CE for the faster-than-Nyquist pilot (FTNP) transmission scenario, where the symbol duration of a pilot block is lower than the Nyquist-criterion-based pilot transmission. Moreover, we propose a serially concatenated channel-encoded FTNS transceiver that takes into account FTNS-specific colored noise effects. The proposed low-complexity receiver carries out soft-decision frequency-domain equalization with the aid of the minimum-mean square error criterion while whitening the colored noise. As explicit benefits of the proposed frequency-domain CE for the FTNP, the demodulated FTNS data block can also be used as a long pilot block, so the iterative joint CE and DD becomes realistic. Simulation results demonstrate that the proposed two-stage-concatenated FTNS system relying on binary phase-shift keying-based FTNP and FTNS-data symbols achieves a better error-ratio performance than previous systems that do not consider colored noise effects in the high-symbol-packing FTNS regime.**

***Index Terms*— Channel estimation, faster-than-Nyquist signaling, frequency-domain equalization, soft-output detection, colored noise, minimum-mean square error, semi-blind detection.**

I. Introduction

THE concept of faster-than-Nyquist signaling (FTNS) was proposed in the 1970s [1], [2]. However, FTNS has recently been rediscovered as a promising technique for next-generation wireless systems, owing to the fact that the FTNS scheme has the potential to achieve higher transmission rates than schemes based on the Nyquist criterion without imposing any bandwidth expansion [3]. In the conventional time-orthogonal Nyquist-criterion scenario, the symbol interval is typically set to not less than $T_0 = 1/(2W)$, where symbols are strictly band-limited to W Hz [4]. Under this assumption, inter-symbol interference (ISI) is not induced in the frequency-flat channel, thereby enabling ISI-free simplified detection [3]. In contrast, in the FTNS scheme, the symbol interval T is typically set to less than T_0, i.e., $T = \alpha T_0$ and $\alpha < 1$, where α is the packing ratio of a symbol. Therefore, in the FTNS scheme, more symbols are transmitted than in the conventional scheme [5]. However, this benefit is achieved at the cost of increased ISI, which imposes a higher demodulation complexity at the receiver.

In order to eliminate the effects of ISI, several time-domain equalizers (TDEs) have been developed for FTNS systems [4]–[7]. The TDE-based FTNS receivers are typically achieved with a high demodulating complexity for a severe ISI scenario with a low α and a long channel tap length. In order to address this problem, low-complexity hard-decision frequency-domain equalization (FDE) was applied to the uncoded FTNS scheme in [8], which relies on diagonal minimum-mean square error (MMSE) demodulation in the frequency domain. The complexity advantage of the FDE-based FTNS receiver over its TDE counterpart is especially noticeable for the high-ISI (high-rate) scenario. Furthermore, the hard-decision FDE of [8] was extended to its soft-decision (SoD) counterpart in [9], which enables practical iterative detection in the channel-encoded FTNS arrangement. This architecture using the powerful channel coding scheme is capable of achieving near-capacity performance, while maintaining a lower complexity, which is the chief benefit of FDE.

However, unlike their TDE counterparts, FDE-based receivers of [8] and [9] did not take into account FTNS-specific colored noise effects [4]–[7], and hence the FDE of [8] and [9] may lead to a performance loss. Most recently, motivated by [8], a hard-decision FDE-based FTNS receiver that considers the effects of colored noise was proposed for uncoded FTNS systems in [10]. In this receiver, the MMSE weights are designed to whiten the FTNS-specific colored noise, where the weight matrix is approximated to be diagonal, in order to maintain low-complexity FDE operation. As a result, the hard-decision FDE of [10] exhibited better BER performance than [8] in the uncoded FTNS scenario. However, since practical FTNS systems typically employ a powerful channel coding scheme [3], such as turbo equalization [11], to eliminate FTNS-specific ISI, it is necessary to consider the iterative FTNS receiver assisted by the SoD demodulator, rather than the hard-decision version of [10] for the sake of practical performance characterization of FTNS.

Manuscript received November 11, 2016; revised March 28, 2017 and June 19, 2017; accepted June 19, 2017. Date of publication July 4, 2017; date of current version September 8, 2017. This work was supported by the Japan Society for the Promotion of Science KAKENHI under Grant 26630170, Grant 26709028, and Grant 16KK0120. This paper was presented at the IEEE ICC, Kuala Lumpur, Malaysia, 2016. The associate editor coordinating the review of this paper and approving it for publication was E. A. Jorswieck. *(Corresponding author: Shinya Sugiura.)*

The authors are with the Department of Computer and Information Sciences, Tokyo University of Agriculture and Technology, Koganei 184-8588, Japan (e-mail: t.ishihara@ieee.org; sugiura@ieee.org).

Color versions of one or more of the figures in this paper are available online at http://ieeexplore.ieee.org.

Digital Object Identifier 10.1109/TWC.2017.2721367

In previous FTNS studies, the perfect channel state information (CSI) was typically assumed to be available at the receiver for the sake of simplicity, except for the studies in the context of spectrally efficient frequency division multiplexing systems [12]–[14]. Naturally, the periodical transmission of Nyquist-based pilot symbols is a simple solution for estimating channel coefficients. In the context of the classic single-carrier transmissions based on the Nyquist criterion, diverse pilot-aided channel estimation (CE) schemes have been developed [15]–[20]. For example, the frequency-domain CE [15]–[18] is a promising low-complexity technique. Furthermore, in [19] and [20], the frequency-flat fading channels and the data symbols are iteratively estimated, where the estimated data symbols are used as the long pilot sequence in order to reduce the mean square errors (MSEs) of the first channel estimation carried out by the original pilot symbols. As explicit benefits of the iterative process, the achievable BER performance becomes very close to that attainable by the perfect CSI assumption. However, this iterative CE and data detection (DD) scheme [19], [20] is not readily applicable to the single-carrier FTNS scenario because CE based on the faster-than-Nyquist pilot (FTNP) sequence is an open issue. Furthermore, the design of the FTNP sequence for the single-carrier FTNS has not been provided.

Against the above-mentioned backdrop, the novel contributions of the present paper are as follows.

- We first propose a low-complexity CE scheme based on the FTNP sequence transmitted from the transmitter. In the derivation of the proposed FTNP-based CE, the detrimental effects of FTNP-specific colored noise are eliminated by proposing an approximated noise-whitening algorithm, which is achieved without imposing any substantial complexity increase. In addition, we provide the design guideline of the single-carrier FTNP sequence, which improves the achievable CE performance.
- Motivated by the FDE developed for the uncoded FTNS, we propose a SoD FDE-based FTNS receiver, which takes into account the effects of colored noise.[1] We demonstrate that the multi-stage-encoded FTNS system using the proposed noise-whitening SoD demodulator exhibits better BER performance than the previous SoD FDE scheme [9] for a low-α scenario, while maintaining a comparable demodulating complexity.
- Moreover, we propose the iterative joint semi-blind FTNP-based CE and DD of uncoded FTNS,[2] which operates in the frequency domain. More specifically, as the explicit benefits of the above-mentioned frequency-domain FTNP-based CE, the demodulated FTNS symbols are exploited as a long pilot sequence in the iterative CE and DD process. Hence, the accuracy of the CE improves upon increasing the number of iterations.
- Furthermore, the above-mentioned joint iterative CE and DD scheme considered in the uncoded FTNS scenario is extended to the two-stage-encoded FTNS scenario. At the receiver, three SoD decoders, i.e., the CE block, the SoD FDE, and the SoD channel decoder, exchange information, hence exploiting the near-capacity and CE-error-free performance.[3]

The remainder of the present paper is organized as follows. In Section II, we present the system model of the proposed FDE-aided FTNS system, and propose the SoD FDE-aided FTNS demodulator that takes into consideration the colored noise. In Section III, we introduce the frequency-domain CE based on the FTNP sequence, as well as the design guideline of the FTNP sequence. Furthermore, the joint iterative CE and DD of uncoded and channel-encoded FTNS systems were presented in Sections IV and V, respectively. Section VI provides the CE and error-rate performance results of the proposed scheme. Finally, we conclude the present paper in Section VII.

Notation: The bold uppercase and lowercase letters represent matrices and column vectors, respectively. Moreover, $\mathbf{Q}_N$ denotes the normalized $(N \times N)$ discrete Fourier transform (DFT) matrix, the lth-row and kth-column element of which is defined as $(1/\sqrt{N})\exp[-2\pi j(k-1)(l-1)/N]$, and $\mathbf{x}_f = \mathbf{Q}_N\mathbf{x}$ denotes the frequency-domain counterpart of the time-domain vector $\mathbf{x}$. The superscript * indicates conjugate operation.

II. System Model

In this section, we introduce the system model of the FTNS transmitter and its FDE-aided FTNS receiver [8], [10] in the uncoded scenario experiencing the additive white-Gaussian noise (AWGN) channel. Then, the system model is extended to the frequency-selective Rayleigh fading channel [9]. Although we assume the use of binary phase-shift keying (BPSK) modulation scheme throughout the paper for simplicity, the extension to the multilevel modulation schemes [22] are readily applicable.

A. Noise-Whitening-FDE-Aided FTNS System in AWGN Channels

Fig. 1 shows the system model of the FDE-aided FTNS structure. At the transmitter, M information bits $\mathbf{b} = [b_0, \cdots, b_{M-1}] \in \mathbb{Z}^M$ are modulated to an N complex-valued symbol vector $\mathbf{s} = [s_0, \cdots, s_{N-1}]^T \in \mathbb{C}^N$. Furthermore, a 2ν-length cyclic prefix (CP), which contains the first 2ν elements of $\mathbf{s}$, is inserted at the end of $\mathbf{s}$. Then, the total $(N+2\nu)$-length symbols are passed through a shaping filter $a(t)$. Throughout the present paper, we assume a root raised cosine (RRC) filter having a roll-off factor β as the shaping filter.[4]

[1] The SoD FDE-based FTNS receiver was originally introduced in a preliminary study [21]. Further novel contributions of this paper over [21] is that we propose the CE for the FTNP scenario, provide the design guideline of the FTNP sequence, and introduce the joint iterative CE and DD. Furthermore, iterative detection between the CE block and SoD decoders of serially concatenated codes is an additional novel contribution of the present paper.

[2] The terminology of *semi-blind* CE indicates that the pilot overhead imposed by CE is maintained to be minimum, which is achieved as the explicit benefit of the joint CE and DD, similar to [19] and [20].

[3] In this paper, we focused our attention on the scenarios of single-carrier FTNS transmissions. The extension of the symbol-packing concept to both the time and the frequency domains is left for the future investigations.

[4] In this paper, we focus our attention on the use of a root raised cosine filter, similar to the previous FTNS studies [3]–[7], [9]. Optimizing the shaping filter is beyond the scope of this paper, which is left for the future study.

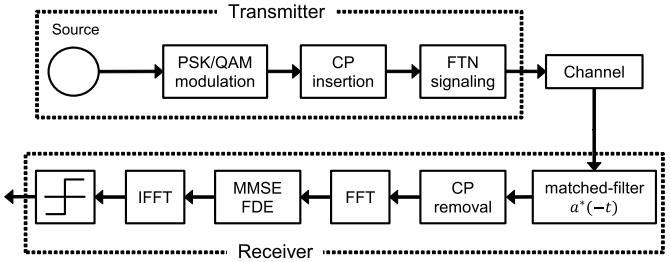

Fig. 1. System model of the FDE-aided FTNS scheme.

Finally, the band-limited symbols are transmitted with an FTNS symbol interval of $T = \alpha T_0$.

At the receiver, the received signals matched-filtered by $a^*(-t)$ are represented as

$$y(t) = \sum_n s_n g(t - nT) + \eta(t), \tag{1}$$

where we have $g(t) = \int a(\tau)a^*(\tau - t)d\tau$ and $\eta(t) = \int n(\tau)a^*(\tau - t)d\tau$, while $n(t)$ represents a random variable that obeys the zero-mean complex-valued Gaussian distribution $\mathcal{CN}(0, N_0)$ with noise variance N_0. Under the assumption of the perfect timing synchronization between the transmitter and the receiver,[5] the kth received signal sample is given by

$$y_k = y(kT) \tag{2}$$
$$= \sum_n s_n g(kT - nT) + \eta(kT), \tag{3}$$

where the component $\eta(kT)$ is the colored noise having a correlation $E[\eta(mT)\eta^*(nT)] = N_0 g(mT - nT)$ because $g(t)$ is non-orthogonal signal at each FTNS sampling time kT.

By deleting both the first and last ν samples from the $(N + 2\nu)$ received samples, we obtain the N-length received signal block, as follows [8]:

$$\mathbf{y} = [y_0, \cdots, y_{N-1}]^T \in \mathbb{C}^N \tag{4}$$
$$= \mathbf{G}\mathbf{s} + \boldsymbol{\eta}, \tag{5}$$

where $\mathbf{G} \in \mathbb{R}^{N\times N}$ is the circulant filter-response matrix, whereas $\boldsymbol{\eta} = [\eta(0), \eta(T), \cdots, \eta((N-1)T)]^T$ represents the associated colored noise. With the aid of the DFT-based eigenvalue decomposition, we obtain

$$\mathbf{G} = \mathbf{Q}_N^T \boldsymbol{\Lambda} \mathbf{Q}_N^*, \tag{6}$$

where $\boldsymbol{\Lambda}$ is the diagonal matrix that consists of the fast Fourier transform (FFT) of the filter response matrix $\mathbf{G}$. Therefore, the frequency-domain counterpart of the received signals (5) may be expressed as

$$\mathbf{y}_f = \mathbf{Q}_N^* \mathbf{y} \tag{7}$$
$$= \boldsymbol{\Lambda}\mathbf{Q}_N^* \mathbf{s} + \mathbf{Q}_N^* \boldsymbol{\eta}. \tag{8}$$

Here, the ideal MMSE weights that whiten the colored noises are given by [10]:

$$\mathbf{W}_{\text{colored}} = \boldsymbol{\Lambda}^H \left(\boldsymbol{\Lambda}\boldsymbol{\Lambda}^H + \frac{1}{E_s}\mathbf{Q}_N^* E[\boldsymbol{\eta}\boldsymbol{\eta}^H]\mathbf{Q}_N^T \right)^{-1}, \tag{9}$$

[5]The precise timing synchronization between the transmitter and the receiver is attainable based on pilot symbols inserted in a frame [23].

where $E[\cdot]$ represents the expectation operation and E_s is the symbol power. Note that, since the noise components $\boldsymbol{\eta}$ have a non-zero cross correlation, the matrix $\mathbf{Q}_N^* E[\boldsymbol{\eta}\boldsymbol{\eta}^H]\mathbf{Q}_N^T$ of (9) does not have a diagonal structure. This implies that the calculation of the MMSE weights $\mathbf{W}_{\text{colored}}$ is highly complex in comparison to the conventional FDE [8], [9], which ignores the colored noise effects. In order to reduce the calculation complexity, the non-diagonal matrix $\mathbf{W}_{\text{colored}}$ is approximated by the diagonal matrix as follows [10]:

$$\tilde{\mathbf{W}}_{\text{colored}} = \boldsymbol{\Lambda}^H \left(\boldsymbol{\Lambda}\boldsymbol{\Lambda}^H + \frac{N_0}{E_s}\boldsymbol{\Phi} \right)^{-1}, \tag{10}$$

where $\boldsymbol{\Phi}$ is the diagonal matrix

$$\boldsymbol{\Phi} = \text{diag}(\Phi[0], \ldots, \Phi[N-1]), \tag{11}$$

while we have

$$\Phi[n] = \frac{1}{N}\sum_{l=0}^{N-1}\sum_{m=0}^{N-1} g((l-m)T) \times \exp\left(j\frac{2\pi(l-m)n}{N} \right). \tag{12}$$

Here, $N_0\Phi[n]$ is the nth diagonal element of matrix $\mathbf{Q}_N^* E[\boldsymbol{\eta}\boldsymbol{\eta}^H]\mathbf{Q}_N^T$ of (9), and $N_0\boldsymbol{\Phi}$ is the power spectral density (PSD) of the colored noise. For comparison, the conventional MMSE weights that ignore the colored noise effects, are represented as [8]

$$\mathbf{W}_{\text{white}} = \boldsymbol{\Lambda}^H \left(\boldsymbol{\Lambda}\boldsymbol{\Lambda}^H + \frac{N_0}{E_s}\mathbf{I}_N \right)^{-1}, \tag{13}$$

where $\mathbf{I}_N$ is the $N \times N$ identity matrix.

Finally, the time-domain symbol estimates $\hat{\mathbf{s}}$ are obtained as

$$\hat{\mathbf{s}} = \mathbf{Q}_N^T \tilde{\mathbf{W}}_{\text{colored}} (\boldsymbol{\Lambda}\mathbf{Q}_N^* \mathbf{s} + \mathbf{Q}_N^* \boldsymbol{\eta}). \tag{14}$$

The spectral efficiency of the FDE-aided FTNS system is given by

$$R = \frac{N}{N + N_r} \cdot \frac{\log_2 \mathcal{M}}{\alpha(1+\beta)} \quad [\text{bits/s/Hz}], \tag{15}$$

where $\mathcal{M}$ is a constellation size, and N_r is the number of CP symbols. Note that, by using a sufficiently long block length N, the normalized overhead of $N_r/(N + N_r)$ imposed by the CP becomes negligible. The demodulation complexity when considering the colored noise will be discussed later herein along with the joint iterative CE and DD schemes proposed in Section IV.

B. Extension to the Frequency-Selective Fading Channels

Let us now extend the AWGN channel model of the previous section to a model applicable to the frequency-selective fading channel. Consider that the delay spread associated with frequency-selective channels spans over $LT = \alpha L T_0$ and that the L complex-valued tap coefficients are given by h_l $(l = 0, \cdots, L-1)$. Then, let us define the first term of (3) as follows:

$$\bar{y}_k = \sum_{n=-\nu}^{\nu} s_n g(kT - nT). \tag{16}$$

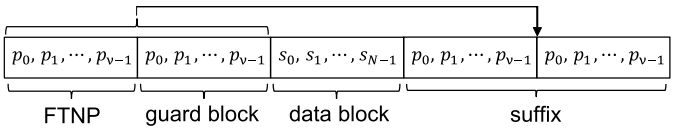

Fig. 2. The frame structure of the proposed FTNS scheme, which consists of the FTNP sequence, the CP, and FTN data symbols.

Hence, the received signals (3) may be rewritten as

$$y_k = \sum_{l=0}^{L-1} h_l \bar{y}_{k-l} + \eta(kT) \tag{17}$$

$$= \sum_{l=0}^{L-1} \sum_{n=-\nu}^{\nu} s_n h_l g(kT - (l+n)T) + \eta(kT). \tag{18}$$

This system model also allows us to have a circulant-matrix-based structure, in the same manner as the matrix $\mathbf{G}$ of (5) in the AWGN channel, by assuming the use of a CP longer than the effective ISI duration. Therefore, the FDE-aided FTNS operation derived in Section II-A is directly applicable to both the frequency-flat and frequency-selective fading scenarios.

However, in these conventional FDE-aided FTNS systems, as well as the TDE-based systems, the perfect CSI acquisition is typically assumed for the sake of the simplicity. In order to address this open issue, we first propose the frequency-domain CE based on the FTNP sequence in the next section.

III. Frequency-Domain CE With an FTNP Sequence

In this section, we first introduce the system model of the FTNP transmissions and then propose the frequency-domain CE algorithm with noise whitening. Finally, we provide the closed-form design guideline of the FTNP sequence.

A. System Model of FTNP Transmission

Fig. 2 shows the transmission frame structure that includes the FTNP sequence, CP, and FTN data symbols. First, the ν-length FTNP sequence of $\mathbf{p} = [p_0, \cdots, p_{\nu-1}]^T$ and a guard block, which is the same as $\mathbf{p}$, are added in advance of the FTNS data block $\mathbf{s}$. Here, this guard block is inserted for the purpose of avoiding the ISI from the FTNP block. The CP is then inserted at the end of the transmission frame such that the entire received frame constructs the circulant matrix structure. Namely, the 2ν-length block $\mathbf{u} = [\mathbf{p}^T, \mathbf{p}^T]^T$ is added both at the beginning and at the end of the data block $\mathbf{s}$. Hence, each frame is composed of the $(N + 4\nu)$-length FTN symbols $\bar{\mathbf{s}} = [\mathbf{u}^T, \mathbf{s}^T, \mathbf{u}^T]^T$, where an additional 2ν-length pilot overhead is imposed on the conventional FDE-aided FTNS [8]. We consider that each frame is transmitted to the receiver over the frequency-selective fading channels.

At the receiver, the first ν samples of the ith frame are used for the CE. Here, we assume that the length ν of the FTNP sequence is sufficiently longer than the delay spread L and that the CIRs remain constant over two successive transmission frames. Then, owing to the guard block of the ith frame as well as the CP of the $(i-1)$st frame, the kth received signal corresponding to the FTNP block $\mathbf{y}_p = [y_{p,0}, \cdots, y_{p,\nu-1}]^T \in \mathbb{C}^\nu$ is represented as follows:

$$\begin{aligned} y_{p,k} = &\sum_{l=0}^{L-1} \sum_{n=0}^{\nu-1} p_n h_l g(kT - (l+n)T) \\ &+ \sum_{l=0}^{L-1} \sum_{n=0}^{\nu-1} p_n h_l g(kT - (l+n+\nu)T) \\ &+ \sum_{l=0}^{L-1} \sum_{n=0}^{\nu-1} p_n h_l g(kT - (l+n-\nu)T) + \eta_p(kT), \end{aligned} \tag{19}$$

where $\eta_p(kT)$ is the corresponding AWGN component. The first term of (19) corresponds to the FTNP symbols of interest and the ISI caused within the block. The second term represents the ISI arising from the ith guard block. Furthermore, the third term denotes the interblock interference (IBI) components induced by the CP of the $(i-1)$st frame.

Based on (19), the received FTNP block $\mathbf{y}_p$ are modified to the circulant-matrix-based representation as follows:

$$\mathbf{y}_p = \mathbf{H}\mathbf{p} + \boldsymbol{\eta}_p \in \mathbb{C}^\nu \tag{20}$$

$$= \mathbf{Q}_\nu^* \boldsymbol{\Lambda}_p \mathbf{Q}_\nu^T \mathbf{p} + \boldsymbol{\eta}_p, \tag{21}$$

where we have

$$\mathbf{H} = \mathbf{Q}_\nu^* \boldsymbol{\Lambda}_p \mathbf{Q}_\nu^T. \tag{22}$$

Note that, since $\mathbf{H}$ is the circulant matrix, the eigenvalue decomposition of (22) is carried out in a manner similar to (6). Moreover, $\boldsymbol{\eta}_p$ are the ν-length colored noise components. Furthermore, $\boldsymbol{\Lambda}_p$ is the $(\nu \times \nu)$-sized diagonal matrix having the diagonal elements $\mathbf{g}_{h,f}$ that are obtained by the FFT of the vector $\mathbf{g}_h = \mathbf{G}_p \mathbf{h}_p$. Here, $\mathbf{G}_p$ is the circulant matrix, represented by the vector $[g(-\nu T) + g(0) + g(\nu T), g((\nu-1)T) + g(-T), g((\nu-2)T) + g(-2T), \cdots, g(T) + g((-\nu+1)T)]^T \in \mathbb{C}^\nu$, while $\mathbf{h}_p = [h_0, h_1, \cdots, h_{L-1}, 0, \cdots, 0]^T \in \mathbb{C}^\nu$ represents the channel coefficients.

B. Frequency-Domain CE With Noise Whitening

In order to carry out frequency-domain CE, the time-domain received signals (21) are modified with the aid of the FFT to

$$\mathbf{y}_{p,f} = \mathbf{Q}_\nu \mathbf{y}_p \tag{23}$$

$$= \boldsymbol{\Lambda}_p \mathbf{p}_f + \boldsymbol{\eta}_{p,f}, \tag{24}$$

where we have

$$\mathbf{p}_f = \mathbf{Q}_\nu^T \mathbf{p}, \tag{25}$$

$$\boldsymbol{\eta}_{p,f} = \mathbf{Q}_\nu \boldsymbol{\eta}_p. \tag{26}$$

Since $\boldsymbol{\Lambda}_p$ is a diagonal matrix, (24) is rewritten as [16]

$$\mathbf{y}_{p,f} = \mathbf{P}\mathbf{g}_{h,f} + \boldsymbol{\eta}_{p,f}, \tag{27}$$

where $\mathbf{P} = \mathrm{diag}\{\mathbf{p}_f\}$. Furthermore, since $\mathbf{g}_{h,f}$ is given by $\mathbf{g}_{h,f} = \sqrt{\nu}\mathbf{Q}_\nu \mathbf{g}_h$, (27) is further modified to obtain

$$\mathbf{y}_{p,f} = \mathbf{P}\sqrt{\nu}\mathbf{Q}_\nu \mathbf{g}_h + \boldsymbol{\eta}_{p,f} \tag{28}$$

$$= \sqrt{\nu}\mathbf{P}\mathbf{Q}_\nu \mathbf{G}_p \mathbf{h}_p + \boldsymbol{\eta}_{p,f} \tag{29}$$

$$= \sqrt{\nu}\mathbf{P}\mathbf{Q}_\nu \mathbf{Q}_\nu^* \boldsymbol{\Lambda}_g \mathbf{Q}_\nu \mathbf{h}_p + \boldsymbol{\eta}_{p,f} \tag{30}$$

$$= \sqrt{\nu}\boldsymbol{\Gamma}\mathbf{Q}_\nu \mathbf{h}_p + \boldsymbol{\eta}_{p,f}, \tag{31}$$

where we have $\mathbf{\Gamma} = \mathbf{P}\mathbf{\Lambda}_g$. Hence, the time-domain channel estimate $\hat{\mathbf{h}}_p$ is obtained with the aid of MMSE filtering as follows:

$$\hat{\mathbf{h}}_p = \frac{1}{\sqrt{\nu}}\mathbf{Q}_\nu^* \mathbf{W}_p \mathbf{y}_{p,f}. \tag{32}$$

By solving the following MMSE problem

$$\begin{aligned}&\arg\min_{\mathbf{W}_p} E[||\mathbf{h}_p - \hat{\mathbf{h}}_p||^2] \\ &\quad = \arg\min_{\mathbf{W}_p} E\left[\left|\left|\mathbf{h}_p - \frac{1}{\sqrt{\nu}}\mathbf{Q}_\nu^*\mathbf{W}_p\mathbf{y}_{p,f}\right|\right|^2\right], \end{aligned}\tag{33}$$

the MMSE weights $\mathbf{W}_p$ are obtained as

$$\mathbf{W}_p = \mathbf{\Gamma}^H\left(\mathbf{\Gamma}\mathbf{\Gamma}^H + \frac{N_0}{\sigma_p}\mathbf{\Phi}_p\right)^{-1}, \tag{34}$$

where $\sigma_p = \sigma_h \cdot \nu$ and $E[\mathbf{h}_p\mathbf{h}_p^H] = \mathbf{R}_h = \sigma_h\mathbf{I}_\nu$. Furthermore, σ_h represents the average power of channel coefficients.

Finally, the CSI estimates $\hat{\mathbf{h}} = [\hat{h}_0, \cdots, \hat{h}_{L-1}]$ are obtained from the first L elements of $\hat{\mathbf{h}}_p$.

C. Design Guideline of the FTNP Sequence

The explicit advantage of the frequency-domain CE expressed in (32) is its low complexity. More specifically, each channel coefficient is calculated as follows:

$$\begin{aligned}\hat{h}_{p,f}[n] &= \frac{\gamma[n]^*}{|\gamma[n]|^2 + \frac{N_0}{\sigma_p}\Phi_p[n]} y_{p,f}[n] \qquad (35)\\ &= \frac{|\gamma[n]|^2}{|\gamma[n]|^2 + \frac{N_0}{\sigma_p}\Phi_p[n]} H[n] \\ &\quad + \frac{\gamma[n]^*}{|\gamma[n]|^2 + \frac{N_0}{\sigma_p}\Phi_p[n]}\eta_{\nu,f}[n], \qquad (36)\end{aligned}$$

where $\gamma[n]$ and $H[n]$ are the nth diagonal element of $\mathbf{\Gamma}$ and the nth element of $\mathbf{Q}_\nu\mathbf{h}_p$, respectively. Note that when $\gamma[n] = 0$, as can be seen from the first term of (36), the channel coefficient $\hat{h}_{p,f}[n]$ is not correctly estimated. In addition, when $\gamma[n]$ has a near-zero value, the CE may suffer from noise-enhancement effects at high SNRs, as seen in the second term of (36). The CE errors in the frequency domain typically spread over other channel coefficients, when $\hat{\mathbf{h}}_{p,f}$ is transformed to the time-domain counterpart.

The classic Nyquist-based frequency-domain CE also suffers from the same detrimental effect. Chu's sequence [24] is typically used to mitigate the CE errors [16], [18]. More specifically, Chu's sequence $\mathbf{c} = [c_1, \cdots, c_\nu]^T$ is represented as [24]

$$c_n = \begin{cases} e^{j\pi kn^2/\nu} & \text{for even } \nu \\ e^{j\pi kn(n+1)/\nu} & \text{for odd } \nu, \end{cases} \tag{37}$$

where ν and k are relatively prime. Note that each pilot symbol c_n has a constant unit amplitude both in the frequency domain and in the time domain, i.e., $|c_n|^2 = |c_{n,f}|^2 = 1$. However, Chu's sequence is not directly applicable to the FTNP scenario, due to the FTNS-specific ISI. That implies that when Chu's sequence is employed as the FTNP sequence, $|\gamma[n]|^2$ is not maintained to be unity, due to the presence of $\mathbf{\Lambda}_g$.

Hence, we propose a novel FTNP design guideline. More specifically, the FTNP sequence is designed based on the criterion that minimizes the MSE of the channel estimates $\hat{\mathbf{h}}_{p,f}$, which is represented by

$$\begin{aligned}\sigma_{\hat{\mathbf{h}}_{p,f}} &= E[||\mathbf{h}_{p,f} - \hat{\mathbf{h}}_{p,f}||^2] \\ &= E\left[\left|\left|\mathbf{h}_{p,f} - \frac{1}{\sqrt{\nu}}\mathbf{W}_p\mathbf{y}_{p,f}\right|\right|^2\right] \\ &\simeq \mathrm{tr}\big\{\mathbf{R}_h - \mathbf{R}_h\mathbf{\Gamma}^H\mathbf{W}_p^H - \mathbf{W}_p\mathbf{\Gamma}\mathbf{R}_h \\ &\quad + \mathbf{W}_p\mathbf{\Gamma}\mathbf{R}_h\mathbf{\Gamma}^H\mathbf{W}_p^H + \frac{1}{\sqrt{\nu}}\mathbf{W}_p\mathbf{\Phi}_p\mathbf{W}_p^H\big\}, \end{aligned}\tag{38}$$

where $\mathrm{tr}\{\cdot\}$ denotes the trace operation. Furthermore, we assumed $E[\mathbf{h}_{p,f}\mathbf{h}_{p,f}^H] = \mathbf{Q}_\nu E[\mathbf{h}_p\mathbf{h}_p^H]\mathbf{Q}_\nu^H = \mathbf{R}_h = \sigma_h\mathbf{I}_\nu$ and $E[\mathbf{W}_p\boldsymbol{\eta}_{p,f}\boldsymbol{\eta}_{p,f}^H\mathbf{W}_p^H] \simeq \mathbf{W}_p\mathbf{\Phi}_p\mathbf{W}_p^H$. Since $\mathbf{W}_p$ and $\mathbf{\Gamma}$ are the real-valued diagonal matrices, we have the relationship of $\mathbf{W}_p\mathbf{\Gamma} = (\mathbf{W}_p\mathbf{\Gamma})^H$. Then, by letting $\mathbf{U} = \mathbf{W}_p\mathbf{\Gamma}$, (38) is simplified to:

$$\sigma_{\hat{\mathbf{h}}_{p,f}} \simeq \mathrm{tr}\big\{\mathbf{R}_h - 2\sigma_h\mathbf{U} + \sigma_h\mathbf{U}^2 + \frac{1}{\sqrt{\nu}}\mathbf{W}_p\mathbf{\Phi}_p\mathbf{W}_p\big\}. \tag{39}$$

The FTNP sequence is obtained by the exhaustive search of the symbol sequence, which minimizes the channel MSE of (39). In our simulations, BPSK symbols are assumed for the FTNP sequence.

IV. Joint Iterative CE and DD in the Uncoded FTNS Scenario

Having developed the CE for the FTNP transmission, let us propose the joint iterative CE and DD of the uncoded FTNS, which is achieved only with the aid of FTNP-based CE.

A. Joint Iterative CE and DD

First, the initial channel estimates $\hat{\mathbf{h}}$ are obtained according to the frequency-domain CE of the FTNP sequence, as introduced in Section III.

Next, DD of the FTNS data block is carried out, according to the frequency-domain FDE. More specifically, by deleting the first and last ν received signals from the $(N+4\nu)$-length signals, the time-domain received signals $\mathbf{r} \in \mathbb{C}^{N+2\nu}$ are represented by

$$\mathbf{r} = \mathbf{G}_x\mathbf{x} + \boldsymbol{\eta}_x. \tag{40}$$

The frequency-domain counterpart of (40) is given by

$$\begin{aligned}\mathbf{r}_f &= \mathbf{D}\mathbf{r} &(41)\\ &= \mathbf{\Lambda}_x\mathbf{D}^T\mathbf{x} + \mathbf{D}\boldsymbol{\eta}_x &(42)\\ &= \mathbf{\Lambda}_x[\mathbf{D}_m \ \ \mathbf{D}_s]\begin{bmatrix}\mathbf{m}\\ \mathbf{s}\end{bmatrix} + \boldsymbol{\eta}_{x,f}, &(43)\end{aligned}$$

where $\mathbf{D} = \mathbf{Q}_{N+2\nu}$, $\mathbf{D}_m$, and $\mathbf{D}_s$ are the submatrices of $\mathbf{D}^T$ having 2ν and N columns, respectively. Since the receiver uses the block $\mathbf{u}$ and the channel estimates $\mathbf{\Lambda}_x$, the ISI imposed

on the data block is eliminated by subtracting $\mathbf{\Lambda}_x\mathbf{D}_m\mathbf{m}$ from (43) as follows [17]:

$$\bar{\mathbf{r}}_f = \mathbf{r}_f - \mathbf{\Lambda}_x\mathbf{D}_m\mathbf{m} \tag{44}$$

$$= \mathbf{\Lambda}_x\mathbf{D}_s\mathbf{s} + \boldsymbol{\eta}_{x,f} \tag{45}$$

$$= \mathbf{\Lambda}_x\mathbf{D}\mathbf{z} + \boldsymbol{\eta}_{x,f}, \tag{46}$$

where we have $\mathbf{z} = [0, \cdots, 0, s_0, \cdots, s_{N-1}]^T \in \mathbb{C}^{N+2\nu}$. Then, the MMSE-FDE operation is carried out as follows:

$$\hat{\mathbf{z}} = \mathbf{D}^*\mathbf{\Lambda}_x\left(\mathbf{\Lambda}_x\mathbf{\Lambda}_x^H + \frac{N_0}{E_s}\mathbf{\Phi}_x\right)^{-1}\bar{\mathbf{r}}_f. \tag{47}$$

Finally, the data symbols $\hat{\mathbf{s}}$ are estimated from the last N elements of $\hat{\mathbf{z}}$.

The accuracy of the initial CE of (32) may not be sufficiently high, due to the minimum size of the FTNP sequence or the low-SNR environment. In order to improve the CE performance, iterative joint CE and DD is carried out. More specifically, the detected data block $\hat{\mathbf{s}}$ is considered to be a long FTNP sequence, and so it is used to update the estimated channels. This is achieved as an explicit benefit of the proposed FTNP-sequence-based CE, iterative joint CE and DD can be performed. The frequency-domain received signals of (42) are expressed as

$$\mathbf{r}_f = \sqrt{N+2\nu}\mathbf{X}\bar{\mathbf{\Lambda}}_g\mathbf{D}\mathbf{h}_x + \boldsymbol{\eta}_{x,f}$$

$$= \rho\mathbf{\Gamma}_x\mathbf{D}\mathbf{h}_x + \boldsymbol{\eta}_{x,f}, \tag{48}$$

where $\rho = \sqrt{N+2\nu}$, $\mathbf{X} = \mathrm{diag}\{\mathbf{x}\}$, $\mathbf{\Gamma}_x = \mathbf{X}\bar{\mathbf{\Lambda}}_g$, and $\mathbf{h}_x = [h_0, h_1, \cdots, h_{L-1}, 0, \cdots, 0]^T \in \mathbb{C}^{N+2\nu}$. Moreover, the diagonal elements of $\bar{\mathbf{\Lambda}}_g$ is given by the FFT coefficients of the circulant matrix $\bar{\mathbf{G}}_x$, whose first column is $[g(-\nu T), 0, \cdots, 0, g(\nu T), g((\nu-1)T), \cdots, g((-\nu+1)T)]^T \in \mathbb{C}^{N+2\nu}$.

Hence, the channel estimates are updated as follows:

$$\hat{\mathbf{h}}_x = \frac{1}{\rho}\mathbf{D}^*\mathbf{\Gamma}_x^H\left(\mathbf{\Gamma}_x\mathbf{\Gamma}_x^H + \frac{N_0}{\sigma_h\rho^2}\mathbf{\Phi}_x\right)^{-1}\mathbf{r}_f, \tag{49}$$

where we obtain the estimated channels $\tilde{\mathbf{h}} = [\tilde{h}_0, \cdots, \tilde{h}_{L-1}]^T$, by extracting the first L elements from $\hat{\mathbf{h}}_x$.

Then, the data symbols are detected again using the updated channel estimates in the same manner as (47). Subsequently, the channel is re-estimated exploiting the re-detected symbols as (49). By performing the above-mentioned iterative CE and DD, the accuracy of the estimated channels and the data symbols are improved upon increasing the number of iterations.

B. Computational Complexity of Proposed Schemes

In this section, we evaluate the computational complexity of the proposed FTNS-based DD, the FTNP-based CE, and the joint iterative CE and DD schemes. First, we discuss the complexity of the SC-FDE scheme with noise whitening, which was introduced in Section II-A. Compared with the previous FDE-aided FTNS scheme [8], which ignores the effects of the colored noise, the only difference is that, in the FDE scheme of (10), $\mathbf{\Phi}$ is added for the purpose of whitening the colored noise. Here, the calculation of $\mathbf{\Phi}$ requires $2N^2$ real-valued multiplications. Therefore, the total cost of $N_0\mathbf{\Phi}$ is the $2N^2$ real-valued and the N complex-valued multiplications. Importantly, $\mathbf{\Phi}$ remains constant for each of the FTNS parameters (α, β) and the block length N, which implies that $\mathbf{\Phi}$ depends only on the shaping filter $h(t)$ and N. Furthermore, $\mathbf{\Phi}$ remains unchanged, irrespective of the presence of fading. Hence, the calculations of $\mathbf{\Phi}$ are stored in the memory of the receiver. Hence, only additional N complex-valued multiplications are required for the calculation of $N_0\mathbf{\Phi}$ in the proposed SC-FDE scheme of (10), in comparison to the conventional scheme [8].

The complexity of the FTNP-based CE of (32) and that of the iterative CE and DD of (47) and (49) are similar to that of the SC-FDE scheme, except that the target block lengths are ν and $(N+2\nu)$, respectively. Moreover, the calculations, imposed on DD of (46), require $(N+2\nu)$ complex-valued multiplications and subtractions.

By expressing DD and CE calculated based on the demodulated data symbols as C_{DD} and C_{rCE}, the total computational complexity of the proposed joint iterative CE and DD becomes $C_{\mathrm{it}} = I_{\mathrm{it}}(C_{\mathrm{DD}} + C_{\mathrm{rCE}}) + C_{\mathrm{DD}}$, where I_{it} is the number of iterations. Therefore, the total complexity C_{it} increases linearly upon increasing the block length $(N+2\nu)$ and the number of iterations I_{it}.

V. SoD FDE-Aided FTNS Detector and Iterative CE and DD for the Two-Stage-Concatenated System

In this section, we first develop the improved SoD FDE-based FTNS detector which considers the colored noise effects, and then provide the two-stage serially concatenated FTNS structure using the proposed FTNS demodulator. Finally, the joint iterative CE and DD is introduced in the channel-encoded scenario.

A. Soft-Decision FDE-Aided FTNS Detection

In the SoD FDE-aided FTNS demodulator, the soft symbols $\tilde{\mathbf{s}} = [\tilde{s}_0, \cdots, \tilde{s}_{N-1}] \in \mathbb{C}^N$ are generated from the *a priori* information that is fed back from the channel decoder. Based on the soft-interference cancellation (SIC) principle [25], the received signals in the time-domain are given by

$$\tilde{\mathbf{y}} = \mathbf{y} - \mathbf{G}\tilde{\mathbf{s}} \tag{50}$$

$$= \mathbf{G}(\mathbf{s} - \tilde{\mathbf{s}}) + \mathbf{n}. \tag{51}$$

Similar to Sections II through IV, the frequency-domain counterparts of (50) are given by

$$\tilde{\mathbf{y}}_f = \mathbf{Q}^*\tilde{\mathbf{y}} = [\tilde{y}_{f,0}, \cdots, \tilde{y}_{f,N-1}]^T \tag{52}$$

$$= \mathbf{\Lambda}\mathbf{Q}_N^*(\mathbf{s} - \tilde{\mathbf{s}}) + \mathbf{Q}_N^*\mathbf{n} \in \mathbb{C}^N. \tag{53}$$

By incorporating the FTNS-induced colored-noise effects into the original SoD SIC-MMSE filtering [26], the frequency-domain symbol estimates $\hat{\mathbf{s}}_f = [\hat{s}_{f,0}, \cdots, \hat{s}_{f,N-1}]^T \in \mathbb{C}^N$ that are obtained by

$$\hat{s}_{f,i} = \frac{\lambda[i]^*}{|\lambda[i]|^2 D + N_0\Phi[i]}\tilde{y}_{f,i}, \tag{54}$$

where $\lambda[i]$ is the ith diagonal element of $\mathbf{\Lambda}$, while D is the reliability value given by $D = -\sum_{i=0}^{N-1}|\tilde{s}_i|^2/N$. Note

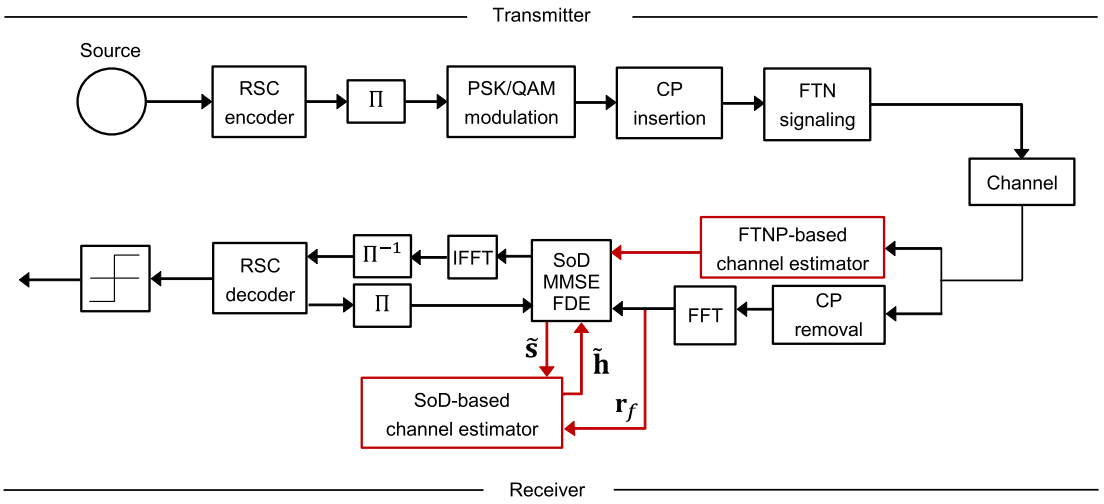

Fig. 3. Transmitter and receiver architectures of the proposed two-stage serially concatenated FTNS system, which is combined with the proposed FTNP-based CE.

that the diagonal approximation is imposed in (54) in order to maintain the low-complexity of FDE. Hence, this may induce a performance loss in comparison to the SoD MMSE-FDE demodulator that uses accurate noise-whitening MMSE weights (9). Nevertheless, we demonstrate in Section VI that the proposed SoD demodulator does not lead to a substantial performance loss. Finally, the time-domain extrinsic log-likelihood ratio (LLR) outputs are calculated as follows [27]:

$$\mathbf{L}_e = [L_e(b_0), \cdots, L_e(b_{N-1})]^T \tag{55}$$

$$= \frac{\rho\tilde{\mathbf{s}} + \mathbf{Q}_N^T\hat{\mathbf{s}}_f}{1+\rho\delta} \in \mathbb{R}^N, \tag{56}$$

where we have

$$\rho = \Re\left[\sum_{i=0}^{N-1} \frac{|\lambda[i]|^2/(|\lambda[i]|^2 D + N_0\Phi[i])}{N}\right] \tag{57}$$

$$\delta = 1 - D. \tag{58}$$

Note that the term $N_0\Phi[i]$ in (54) and (57) is replaced by N_0 in the conventional demodulator [9].

B. Joint Iterative CE and DD for the Two-Stage-Concatenated Channel-Encoded FTNS System

In this section, the joint iterative CE and DD developed for the uncoded FTNS system in Section IV is extended to that supporting the channel-encoded counterpart, in order to achieve near-capacity performance.

Fig. 3 shows the two-stage serially concatenated FTNS transceiver architecture, which relies on the proposed low-complexity SoD FDE-based FTNS demodulator, FTNP-based CE, and iterative processing between the CE and the DD blocks. At the transmitter, information bits are first encoded by the recursive systematic convolutional (RSC) encoder, and the RSC-encoded bits are then interleaved by the interleaver Π. The interleaved bits are modulated onto the FTNS symbols, as shown in Section III.

At the receiver, the joint iterative CE and DD are carried out, as shown in the lower part of Fig. 3. More specifically, the FTNP-based CE block first outputs the initial channel estimates to the SoD MMSE FDE block. At the SoD MMSE FDE block, the LLRs are calculated from the receive signals, the estimated channels, and the extrinsic information gleaned from the RSC decoder, according to (56). Then, the estimated time-domain data symbols $\tilde{\mathbf{s}}$ are deinterleaved and input into the RSC decoder. The RSC decoder outputs the estimated information bits, while exchanging extrinsic information with the SoD MMSE FDE block. In each exchange of extrinsic information between the RCS decoder and FDE, the soft symbols $\tilde{\mathbf{s}}$ are updated in the FDE block, which are input to the SoD-based channel estimator. Then, the channel estimates are updated and fed back into the FDE block. Note that the number of iterations between the FDE block and the RCS decoder (the SoD-based channel estimator) is given by I_t.[6]

Note that upon increasing the iterations between the CE and the iterative decoding, the accuracy of the channel estimates as well as the BER performance improves.

VI. Simulation Results

In order to characterize the achievable performance of a set of the proposed schemes, including the FTNP-based CE, the FDE-aided FTNS DD, and joint iterative CE and DD both in uncoded and channel-encoded scenarios, we investigated the achievable MSE and BER performance. Here, the MSE is defined as $\sum_{n=0}^{L-1}|h_n - \tilde{h}_n|^2$ for the frequency-selective Rayleigh block fading channels.

A. CE Performance

First, Fig. 4 shows the MSE calculated for the proposed FTNP-based CE of Section III and the proposed iterative

[6]Note that naturally, the decoding complexity of the iterative detection linear increases, upon increasing the number of iterations. Moreover, in order to attain the near-capacity performance expected for the channel-encoded systems, a sufficiently long interleaver length is typically required.

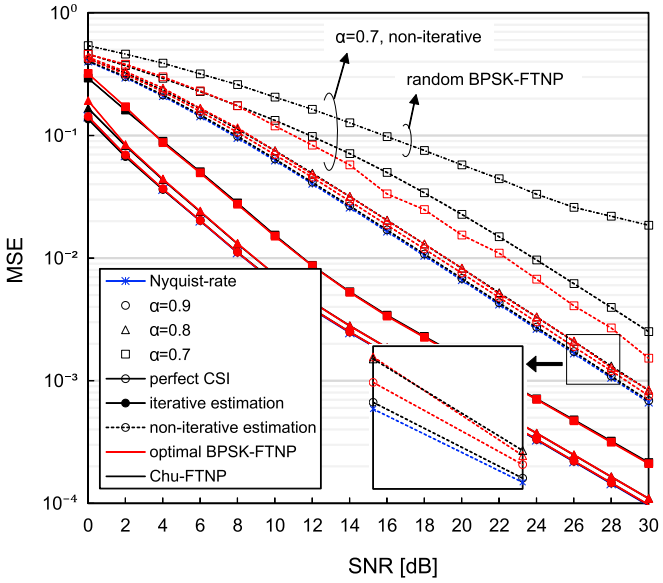

Fig. 4. The MSE performance of the proposed FTNP-based CE scheme and the iterative CE scheme. The FTNS parameters were set to $(\alpha, \beta, \nu) = (0.9, 0.5, 15)$, $(0.8, 0.5, 15)$, and $(0.7, 0.5, 15)$. The delay spread was $L = 10$.

CE and DD scheme of Section IV. We considered both the proposed FTNP sequence and the conventional Chu's one. Moreover, the frequency-selective fading channels having a delay spread of $L = 10$ were considered, while the data-block length N and the number of iterations I_{it} were set to $N = 1024$ and $I_{\text{it}} = 5$, respectively. The FTNS parameters (α, β, ν) were given by $(0.9, 0.5, 15)$, $(0.8, 0.5, 15)$, and $(0.7, 0.5, 15)$, which correspond to the transmission rates of approximately $0.7, 0.8$, and 0.9 [bps/Hz], respectively. In Fig. 4, the MSE bound achievable by the Nyquist-criterion-based Chu-pilot sequence is plotted as a benchmark. As shown in Fig. 4, the proposed CE scheme nearly achieved the same MSEs as the Nyquist-criterion-based CE ($\alpha = 1$) both in the non-iterative and iterative scenarios. Naturally, upon reducing α, the MSEs deteriorated at the cost of the reduced CE overhead. Furthermore, note that the proposed iterative CE and DD scheme exhibited a significantly better MSE performance than its non-iterative counterpart, irrespective of the α value. Also, in the non-iterative CE scenario, the proposed BPSK-based FTNP sequence achieved a better performance than the Chu's sequence with $\alpha = 0.7$, while the proposed BPSK-based sequence exhibited the MSE performance comparable that attained by Chu's sequence for $\alpha = 0.8$ and $\alpha = 0.9$.

In order to elaborate a little further, Fig. 5 shows the MSE performance of CE, which was attained by the proposed BPSK-based FTNP sequence and Chu's sequence [24], where the iterative CE and DD was deactivated. The FTNS parameters were set to $(\alpha, \beta, \nu) = (0.9, 0.1, 15)$, $(0.9, 0.3, 15)$, and $(0.8, 0.3, 15)$, while the delay spread was $L = 10$. Observe in Fig. 5 that the proposed BPSK-based FTNP sequence attained a better performance in a low-β scenario. To be moer specific, since the effects of FTNS-induced ISI become explicit for a low β value, the proposed BPSK-based FTNP sequence outperforms Chu's sequence also in low-α FTNP scenarios.

In order to further evaluate the effects of the number of iterations I_{it}, the MSEs were plotted in Fig. 6 for various

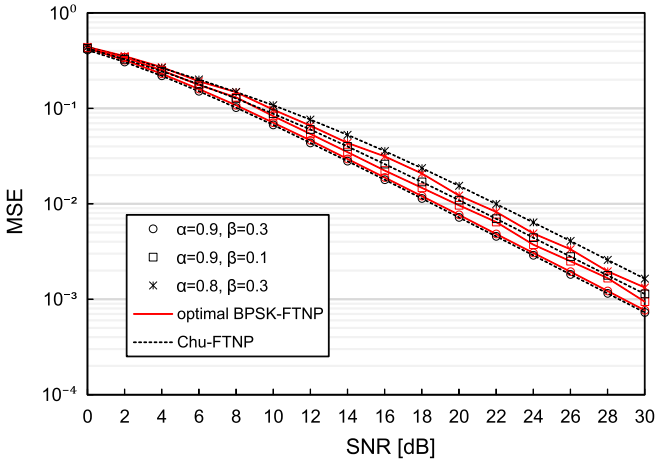

Fig. 5. The MSE performance of CE, which was attained by the proposed BPSK-based FTNP sequence and Chu's sequence [24], where the iterative CE and DD was deactivated. The FTNS parameters were set to $(\alpha, \beta, \nu) = (0.9, 0.1, 15)$, $(0.9, 0.3, 15)$, and $(0.8, 0.3, 15)$, while the delay spread was $L = 10$.

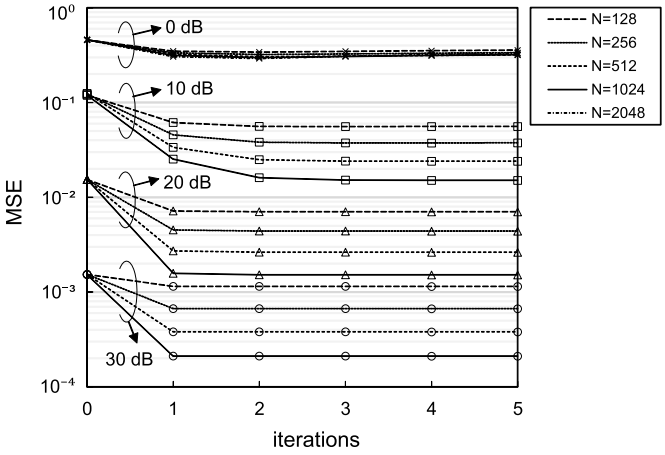

Fig. 6. The MSE of the channel coefficients estimated by the proposed iterative CE and DD system, where the number of iterations was varied from zero to five, and the data block length was given by $N = 128$, 256, 512, and 1024. The SNR was given by 0, 10, 20 and 30 dB. The system parameters were set to $(\alpha, \beta, \nu) = (0.7, 0.5, 15)$ and $L = 10$.

numbers of iterations from $I_{\text{it}} = 0$ to 5, where we had the system parameters of $(\alpha, \beta, \nu) = (0.7, 0.5, 15)$, the block length of $N = 128, 256, 512$, and 1024, as well as the SNRs of 0, 10, 20, and 30 dB. Moreover, the delay spread was given by $L = 10$. In each SNR scenario, the MSE improved upon increasing the number of iterations and converged to a constant value within as few as $I_{\text{it}} = 2$ iterations. Furthermore, the MSE was found to improve, upon increasing the data-block length N because the CE update in the iterative CE and DD became more accurate for the long FTNP sequence. Note that this benefit was especially explicit for high-SNR scenarios.

To provide further insights, in Fig. 7 we investigated the effects of the number of iterations I_{it} and the block length N on the achievable MSE performance, while varying the system parameters of β and ν. For the scenario of $(\alpha, \beta, \nu) = (0.8, 0.3, 11)$, the MSE converged quickly with two iterations,

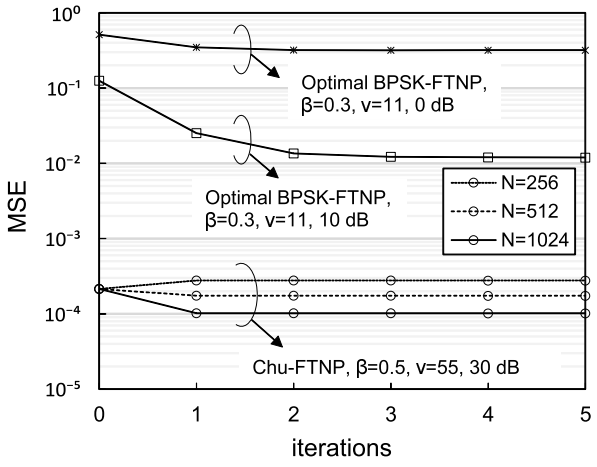

Fig. 7. The effects of the number of iterations $I_{\rm it}$ and of data bolock length N on the achievable MSE performance. The FTNS parameters were set to $(\alpha, \beta, \nu) = (0.8, 0.3, 11)$ and $(0.8, 0.5, 55)$. The delay spread was $L = 10$. The proposed BPSK-based FTNP sequence was employed for SNRs of 0 and 10 dB, while Chu-FTNP sequence was employed for SNR of 30 dB.

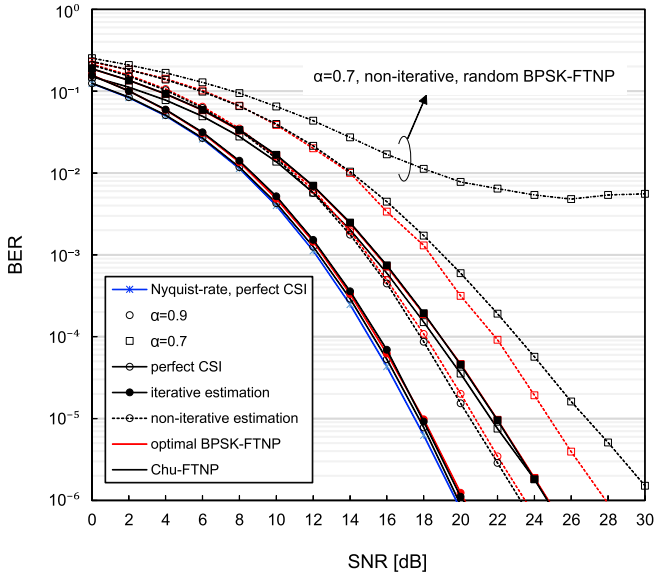

Fig. 8. Achievable BER of the FDE-aided uncoded FTNS systems using the proposed FTNP-based CE scheme and the joint iterative CE and DD scheme, where the FTNS parameters were set to $(\alpha, \beta, \nu) = (0.9, 0.5, 15)$ and $(0.7, 0.5, 15)$. The number of iterations and delay spread were set to $I_{\rm it} = 5$ and $L = 10$, respectively.

which remained unchanged from the results of Fig. 6. By contrast, when we considered a long FTNP-length $4\nu = 220$, which is comparable to the block length, the benefit of the proposed iterative CE and DD scheme disappeared.

B. BER Performance in the Uncoded FTNS Scenario

In Fig. 8, we investigated the achievable BER performance of the joint iterative CE and DD in the uncoded FTNS system of Section IV. The system parameters were given as $(\alpha, \beta, \nu) = (0.9, 0.5, 15)$ and $(0.7, 0.5, 15)$, while the number of iterations between the CE and DD blocks was set to $I_{\rm it} = 5$. For comparisons, we plotted the perfect-CSI

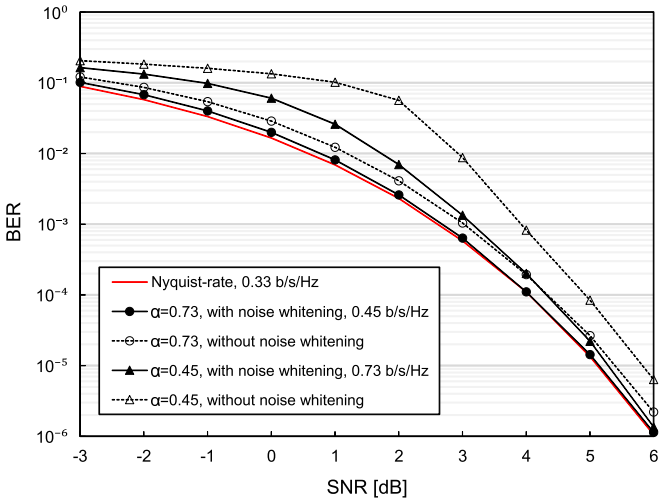

Fig. 9. Achievable BER of the improved SoD FDE-aided two-stage-concatenated FTNS systems in the AWGN channel, where the parameters were set to $(\alpha, \beta, \nu) = (0.73, 0.5, 10)$ and $(0.45, 0.5, 10)$.

bounds both for the Nyquist-criterion-based and the FTNS systems, exploiting FDE at the receiver. In addition to Chu's sequence, the randomly generated BPSK sequence was also employed as a benchmark. As shown in Fig. 8, in each α scenario, the BER curve of the proposed joint iterative CE and DD scheme converged to the perfect-CSI bound, whereas the non-iterative counterpart did not. More specifically, the performance advantage of the proposed scheme over the non-iterative counterpart ($I_{\rm it} = 0$), which was recorded for BER$= 10^{-6}$, was 3 dB for $\alpha = 0.9$ and $\alpha = 0.7$ when employing the proposed BPSK-FTNP sequence. Furthermore, in the non-iterative scenario, the error-floor was induced when the random BPSK-FTNP sequence was used, while the best performance was achieved when using the proposed BPSK-FTNP sequence, which outperformed the conventional Chu's sequence.

C. BER Performance in the Channel-Encoded FTNS Scenario

Finally, as shown in Figs. 9 through 11, we consider the joint iterative CE and DD scheme in the two-stage RSC-encoded FTNS system of Section V. Fig. 9 shows the achievable BER of the two-stage RSC-coded FTNS system calculated using the proposed SoD FDE in the AWGN channel. The system parameters were set to $(\alpha, \beta, \nu) = (0.73, 0.5, 10)$ and $(0.45, 0.5, 10)$, while the half-rate RSC(2,1,2) code having octal generator polynomials of (3,2) was used, and hence the spectrum efficiency is half those considered in the uncoded counterparts. The interleaver length was $2^{17} = 131,072$. We also plotted the Nyquist-criterion bound as well as the BER curves of the conventional SoD FDE [9]. Fig. 9 shows that the BER of the proposed scheme converged to the Nyquist-criterion bound, while achieving better performance than the conventional FDE, which does not whiten the colored noise. Furthermore, the proposed FDE's performance advantage over the conventional FDE [9] increased upon increasing the transmission rate. These results ensure that the proposed noise-whitening FDE does not impose any substantial performance

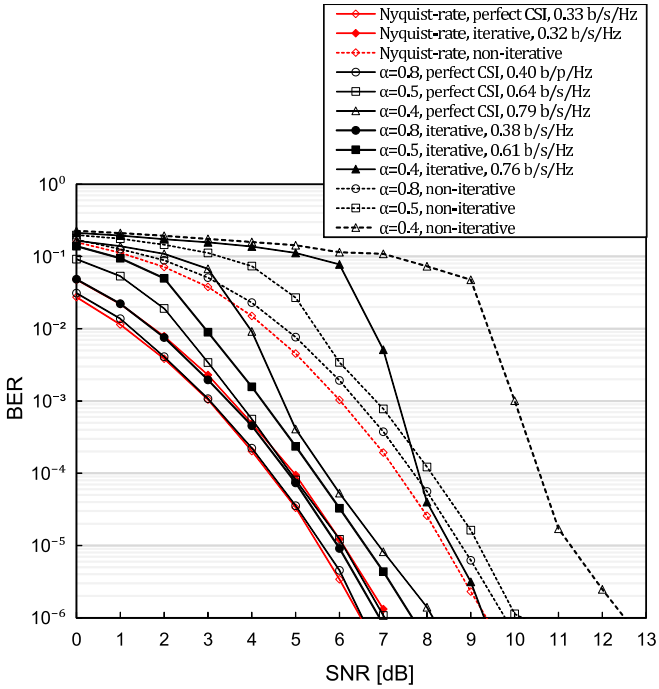

Fig. 10. Achievable BER of the improved SoD FDE-aided two-stage FTNS systems using the proposed FTNP-based CE scheme and joint iterative CE and DD scheme under the frequency-selective Rayleigh block fading channels with $L = 20$, where the parameters were set to $(\alpha, \beta, \nu) = (0.8, 0.5, 25)$, $(0.5, 0.5, 25)$, and $(0.4, 0.5, 25)$, while we have $I_{\rm t} = 21$.

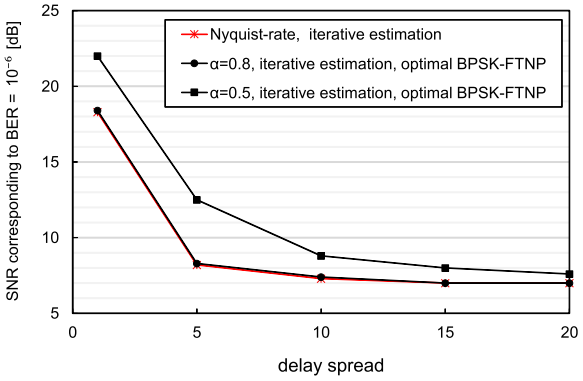

Fig. 11. Signal-to-noise ratio required to achieve a BER of 10^{-6} for each delay spread L in two-stage iterative CE and DD systems. The proposed BPSK-based FTNP sequence having the length of $\nu = 25$ was employed.

loss in the AWGN channel, despite the diagonal approximation used in the derivation of the MMSE weights in (10).

In Fig. 10, we considered the frequency-selective Rayleigh block fading environment, exhibiting the delay spread of $L = 20$. The system parameters were set to $(\alpha, \beta, \nu) = (0.8, 0.5, 25)$, $(0.5, 0.5, 25)$ and $(0.4, 0.5, 25)$, while the interleaver length was $2^{18} = 262,144$. Moreover, the number of iterations between the SoD FDE and the SoD RSC decoder was $I_{\rm t} = 21$. Fig. 10 indicates that the proposed joint iterative CE and DD scheme exhibited better BER performance than its non-iterative-CE counterpart ($I_{\rm it} = 0$), where the performance gains at high SNRs were 2.8 dB, 2.5 dB, and 2.9 dB for $\alpha = 0.8$, 0.5, and 0.4, respectively.

In Fig. 11, we evaluated the effects of the delay spread L on the achievable BER performance of the proposed scheme. More specifically, we investigated the effective SNR, which was recorded for a BER of 10^{-6}, while varying the delay spread from $L = 1$ to 20. The system parameter sets $(\alpha, \beta, \nu) = (0.8, 0.5, 25)$ and $(0.5, 0.5, 25)$ were used. As shown in Fig. 11, the SNR for a low-rate scenario of $\alpha = 0.8$, the effective SNR of the proposed scheme was nearly the same as that of the Nyquist-criterion bound ($\alpha = 1.0$). In contrast, the performance loss for a high-rate scenario of $\alpha = 0.5$, although limited to a couple of decibels, was found when the delay spread was higher than $L = 10$.

VII. Conclusions

In this paper, we proposed the low-complexity frequency-domain CE scheme, based on the FTNP sequence, where the detrimental effects of FTNP-specific colored noise are eliminated as an explicit benefit of an approximated noise-whitening algorithm. Also, the FTNP sequence was designed for improving the achievable CE performance. Furthermore, we proposed the low-complexity SoD FDE-based FTNS receiver, which also considers the effects of colored noise. Moreover, we proposed the iterative joint semi-blind FTNP-based CE and DD of uncoded FTNS, which is achieved as the explicit benefits of the above-mentioned frequency-domain FTNP-based CE. More specifically, the demodulated FTNS symbols are exploited as a long pilot sequence in the iterative CE and DD process. The joint iterative CE and DD scheme considered in the uncoded FTNS scenario was extended to the two-stage RSC-encoded FTNS scenario. At the receiver, three SoD decoders exchange information, hence exploiting the near-capacity and CE-error-free performance, as demonstrated in our simulations.

References

[1] J. Salz, "Optimum mean-square decision feedback equalization," *Bell System Tech. J., The*, vol. 52, no. 8, pp. 1341–1373, Oct. 1973.
[2] J. E. Mazo, "Faster-than-Nyquist signaling," *Bell Syst. Tech. J.*, vol. 54, no. 8, pp. 1451–1462, 1975.
[3] J. B. Anderson, F. Rusek, and V. Öwall, "Faster-than-Nyquist signaling," *Proc. IEEE*, vol. 101, no. 8, pp. 1817–1830, Aug. 2013.
[4] A. D. Liveris and C. N. Georghiades, "Exploiting faster-than-Nyquist signaling," *IEEE Trans. Commun.*, vol. 51, no. 9, pp. 1502–1511, Sep. 2003.
[5] A. Prlja and J. B. Anderson, "Reduced-complexity receivers for strongly narrowband intersymbol interference introduced by faster-than-Nyquist signaling," *IEEE Trans. Commun.*, vol. 60, no. 9, pp. 2591–2601, Sep. 2012.
[6] F. Rusek and J. B. Anderson, "Multistream faster than Nyquist signaling," *IEEE Trans. Commun.*, vol. 57, no. 5, pp. 1329–1340, May 2009.
[7] M. McGuire and M. Sima, "Discrete time faster-than-Nyquist signalling," in *Proc. Global Telecommun. Conf.*, Miami, FL, USA, Dec. 2010, pp. 1–5.
[8] S. Sugiura, "Frequency-domain equalization of faster-than-Nyquist signaling," *IEEE Wireless Commun. Lett.*, vol. 2, no. 5, pp. 555–558, Oct. 2013.
[9] S. Sugiura and L. Hanzo, "Frequency-domain equalization aided iterative detection of faster-than-Nyquist signaling," *IEEE Trans. Veh. Technol.*, vol. 64, no. 4, pp. 2122–2128, Apr. 2015.
[10] H. Fukumoto and K. Hayashi. (Sep. 2015). "Overlap frequency domain equalization for faster-than-Nyquist signaling." [Online]. Available: https://arxiv.org/abs/1509.00562
[11] M. Tuchler, R. Koetter, and A. C. Singer, "Turbo equalization: Principles and new results," *IEEE Trans. Commun.*, vol. 50, no. 5, pp. 754–767, May 2002.

[12] A. Chorti, I. Kanaras, M. R. D. Rodrigues, and I. Darwazeh, "Joint channel equalization and detection of spectrally efficient FDM signals," in *Proc. 21st Annu. IEEE Int. Symp. Pers., Indoor Mobile Radio Commun.*, Sep. 2010, pp. 177–182.
[13] S. Isam and I. Darwazeh, "Robust channel estimation for spectrally efficient FDM system," in *Proc. 19th Int. Conf. Telecommun. (ICT)*, Apr. 2012, pp. 1–6.
[14] T. Xu and I. Darwazeh, "Transmission experiment of bandwidth compressed carrier aggregation in a realistic fading channel," *IEEE Trans. Veh. Technol.*, vol. 66, no. 5, pp. 4087–4097, May 2016.
[15] L. Deneire, B. Gyselinckx, and M. Engels, "Training sequence versus cyclic prefix—A new look on single carrier communication," *IEEE Commun. Lett.*, vol. 5, no. 7, pp. 292–294, Jul. 2001.
[16] J. Coon, M. Beach, and J. McGeehan, "Optimal training sequences for channel estimation in cyclic-prefix-based single-carrier systems with transmit diversity," *IEEE Signal Process. Lett.*, vol. 11, no. 9, pp. 729–732, Sep. 2004.
[17] Y. Zeng and T. S. Ng, "Pilot cyclic prefixed single carrier communication: Channel estimation and equalization," *IEEE Signal Process. Lett.*, vol. 12, no. 1, pp. 56–59, Jan. 2005.
[18] Y. R. Zheng and C. Xiao, "Channel estimation for frequency-domain equalization of single-carrier broadband wireless communications," *IEEE Trans. Veh. Technol.*, vol. 58, no. 2, pp. 815–823, Feb. 2009.
[19] S. Chen, S. Sugiura, and L. Hanzo, "Semi-blind joint channel estimation and data detection for space-time shift keying systems," *IEEE Signal Process. Lett.*, vol. 17, no. 12, pp. 993–996, Dec. 2010.
[20] P. Zhang, S. Chen, and L. Hanzo, "Two-tier channel estimation aided near-capacity MIMO transceivers relying on norm-based joint transmit and receive antenna selection," *IEEE Trans. Wireless Commun.*, vol. 14, no. 1, pp. 122–137, Jan. 2015.
[21] T. Ishihara and S. Sugiura, "Frequency-domain equalization aided iterative detection of faster-than-Nyquist signaling with noise whitening," in *Proc. IEEE Int. Conf. Commun.*, Kuala Lumpur, Malaysia, May 2016, pp. 1–6.
[22] T. Matsumoto, S. Ibi, S. Sampei, and R. Thomä, "Adaptive transmission with single-carrier multilevel BICM," *Proc. IEEE*, vol. 95, no. 12, pp. 2354–2367, Dec. 2007.
[23] C. Herzet *et al.*, "Code-aided turbo synchronization," *Proc. IEEE*, vol. 95, no. 6, pp. 1255–1271, Jun. 2007.
[24] D. C. Chu, "Polyphase codes with good periodic correlation properties," *IEEE Trans. Inf. Theory*, vol. IT-18, no. 4, pp. 531–532, Jul. 1972.
[25] M. Tuchler, A. C. Singer, and R. Koetter, "Minimum mean squared error equalization using *a priori* information," *IEEE Trans. Signal Process.*, vol. 50, no. 3, pp. 673–683, Mar. 2002.
[26] B. Ng, C. T. Lam, and D. Falconer, "Turbo frequency domain equalization for single-carrier broadband wireless systems," *IEEE Trans. Wireless Commun.*, vol. 6, no. 2, pp. 759–767, Feb. 2007.
[27] K. Kansanen and T. Matsumoto, "An analytical method for MMSE MIMO turbo equalizer EXIT chart computation," *IEEE Trans. Wireless Commun.*, vol. 6, no. 1, pp. 59–63, Jan. 2007.

Takumi Ishihara (S'16) received the B.E. and M.E. degrees in computer and information sciences from the Tokyo University of Agriculture and Technology, Tokyo, Japan, in 2016 and 2017, respectively, where he is currently pursuing the Ph.D. degree.

His research interest is in faster-than-Nyquist signaling.

Shinya Sugiura (M'06–SM'12) received the B.S. and M.S. degrees in aeronautics and astronautics from Kyoto University, Kyoto, Japan, in 2002 and 2004, respectively, and the Ph.D. degree in electronics and electrical engineering from the University of Southampton, Southampton, U.K., in 2010.

From 2004 to 2012, he was a Research Scientist with Toyota Central Research and Development Laboratories, Inc., Aichi, Japan. Since 2013, he has been an Associate Professor with the Department of Computer and Information Sciences, Tokyo University of Agriculture and Technology, Tokyo, Japan, where he currently heads the Wireless Communications Research Group. He authored or co-authored over 80 refereed research publications, including 50 IEEE journal and magazine papers. His research has covered a range of areas in wireless communications, networking, signal processing, and antenna technology.

Dr. Sugiura was a recipient of a number of awards, including the Sixth RIEC Award from the Foundation for the Promotion of Electrical Communication in 2016, the Young Scientists' Prize by the Minister of Education, Culture, Sports, Science and Technology of Japan in 2016, the 14th Funai Information Technology Award (First Prize) from the Funai Foundation in 2015, the 28th Telecom System Technology Award from the Telecommunications Advancement Foundation in 2013, the Sixth IEEE Communications Society Asia-Pacific Outstanding Young Researcher Award in 2011, the 13th Ericsson Young Scientist Award in 2011, and the 2008 IEEE Antennas and Propagation Society Japan Chapter Young Engineer Award. He was also certified as an Exemplary Reviewer of IEEE COMMUNICATIONS LETTERS in 2013 and 2014.